



Thermal Spray Coatings for Blast Furnace Tuyere Application

A. Pathak, G. Sivakumar, D. Prusty, J. Shalini, M. Dutta, and S.V. Joshi

(Submitted April 30, 2015; in revised form October 26, 2015)

The components in an integrated steel plant are invariably exposed to harsh working environments involving exposure to high temperatures, corrosive gases, and erosion/wear conditions. One such critical component in the blast furnace is the tuyere, which is prone to thermal damage by splashing of molten metal/slag, erosive damage by falling burden material, and corrosion from the ensuing gases. All the above, collectively or independently, accelerate tuyere failure, which presents a potential explosion hazard in a blast furnace. Recently, thermal spray coatings have emerged as an effective solution to mitigate such severe operational challenges. In the present work, five different coatings deposited using detonation spray and air plasma spray techniques were comprehensively characterized. Performance evaluation involving thermal cycling, hot corrosion, and erosion tests was also carried out. Based on the studies, a coating system was suggested for possible tuyere applications and found to yield substantial improvement in service life during actual field trials.

Keywords blast furnace tuyere, erosion testing, hot corrosion, thermal cycling, thermal spray coating

1. Introduction

Production hardware in an integrated steel plant is always exposed to severe operating environment, which typically involves a combination of high temperature, corrosive gases, and erosion/wear conditions (Ref 1). Such a harsh environment tends to accelerate the rate of degradation and eventually leads to a decrease in product quality, reduction in operating efficiency, invokes greater maintenance cost, and, more significantly, higher overall downtime (Ref 2). One such important hardware is the tuyere used in a blast furnace. Made of copper and necessarily water cooled (Ref 3), it is essentially used for injecting hot air (~1100 °C) and pulverized coal into the furnace. The service life and energy-saving effect of a tuyere have a direct influence over the operating cost of the furnace and productivity of the molten metal.

This article is an invited paper selected from presentations at the 6th Asian Thermal Spray Conference (ATSC 2014) and has been expanded from the original presentation. ATSC 2014 was held in Hyderabad, India, November 24-26, 2014, and was organized by the International Advanced Research Centre for Powder Metallurgy and New Materials (ARCI) and the Asian Thermal Spray Society.

A. Pathak, D. Prusty, and M. Dutta, Research & Development, Tata Steel Ltd., Jamshedpur, India; and G. Sivakumar, J. Shalini, and S.V. Joshi, Centre for Engineered Coatings, ARCI, Hyderabad, India. Contact e-mails: abhishek.pathak@tatasteel.com and pathak.223@gmail.com.

A tuyere typically operates in severe environments, with temperatures in the vicinity reaching around 2000 °C (Ref 4). Although inherently provided with extensive water cooling, a tuyere is prone to severe thermal damage due to (a) sudden rise in temperature through premature combustion of pulverized coal within the tuyere nose and (b) splashing of molten metal and slag on the tuyere nose. Most of the mechanical damage occurs through impact of molten slag and falling feedstock (coke, iron ore, sinter, pellets, etc.) materials. Further damage is also anticipated from corrosive gases like sulfur and chlorine that emanate during burning of coal. Such damage, apart from reducing the efficiency of a tuyere, increases the possibility of explosion within the blast furnace due to ingress of cooling water from the fractured tuyere within the molten metal (Ref 5). Hence, imparting better protection at the ‘nose’ part of tuyere is of significant interest to the steel industry (Ref 6).

Thermal spray coating has been explored as a potential solution to mitigate problems associated with tuyere failure (Ref 7-13). A three-layered system comprising Ni-Co-based self-fluxing bond coat, an intermediate cermet layer, and a top layer of zirconia or alumina by plasma or oxy-acetylene flame spray was found to provide improved thermal shock resistance, and an increase in service life of 50% was also claimed (Ref 7). Further, an addition of Mo, W, and Si elements to the intermediate cermet layer was claimed to improve the interlayer adhesion of the intermediate cermet layer. A top layer comprising a mixture of Zirconia-Alumina-Titania and Silica was found to yield a two- to three-fold increase in service life compared to a conventional TBC system (Ref 8). However, the systems proposed in Ref 7 and 8 did not get wide commercial acceptance due to distortion of copper tuyere at the high temperature required for self-fluxing of the bond coat as well as because of spallation problem of the intermediate cermet layer (Ref 9). Other potential coating solutions

such as in situ tuyere coating by alumina and chromium nitride for improved wear resistance (Ref 10), Cu-Al-Fe aluminized layer formation using diffusion process to increase overall service life of tuyere (Ref 11), and Cu-Al aluminizing on inner and outer surface of tuyere for improved wear resistance (Ref 12) have also been reported. Fukubayashi (Ref 9) reported a TBC system using a Co-based bond coat and zirconia top coat, with an optional boride or carbide top layer, deposited by detonation spray coating (DSC) for improved erosion performance of tuyere, while Song et al. (Ref 13) used a three-layered TBC system with atmospheric plasma-sprayed (APS) Ni bond coat, high velocity oxy-fuel (HVOF)-sprayed NiCrAl intermediate layer, and APS ceramic top coat comprising YSZ and alumina for higher tuyere life. The above efforts were all focused on a single specific mode of degradation (e.g., thermal shock or wear) and resulted only in marginal improvement in service life of tuyere. As discussed earlier, actual tuyere failure is caused by multiple mechanisms; hence, there is a clear need for a comprehensive assessment to identify a more robust coating solution to suitably combat all possible problems associated with tuyere degradation.

The present manuscript highlights results from an elaborate exercise undertaken to address the above need. Two prominent thermal spray variants, namely detonation spray coating (DSC) and atmospheric plasma spraying (APS), and five different material systems were identified as prospective candidates for protecting the tuyeres. The choice of DSC has been dictated by its ability to yield highly dense and well-adherent coatings, without any significant in situ thermal damage to the powder feedstock due to oxidation, phase change, etc. (Ref 14). APS was also chosen because of its wide industrial acceptance for deposition of coatings for high temperature applications (Ref 2). All generated coatings were comprehensively characterized and also tested for different forms of degradation typically experienced by a tuyere in actual operation. Although many different materials have been individually studied by various thermal spray techniques in the past, the present study is unusual in that it undertakes an expansive study to enable a comparison of properties of all the chosen coating materials by both deposition techniques, possibly for the first time, to identify the most appropriate coating material-coating process combination to address an application of significant industry interest. Based on the ensuing results, the coatings were ranked and the most promising coating was chosen to be applied on an actual blast furnace tuyere for field evaluation in a real oper-

ating environment. The outcome of the field trials is also discussed herein.

2. Experimental Procedure

2.1 Coating and Substrate Materials

Five candidate coatings, namely Yttria-stabilized Zirconia (YSZ), Cr₃C₂-25NiCr (CrC), YSZ+20% mullite (M-YSZ), mullite (M), and Al₂O₃-ZrO₂ (AZ), were chosen based on their ready commercial availability, potential to impart suitable protection to the tuyeres as well as based on cost considerations for eventual implementation in the plant. The powders used in the present study were procured from various sources: Yttria-stabilized Zirconia from Sulzer Metco, USA, Cr₃C₂-25NiCr from Praxair, USA, and mullite and Al₂O₃-ZrO₂ from Saint Gobain, USA. In case of YSZ+20 wt.% mullite, the individual powders were separately weighed and mechanically mixed in a rotary ball mill for 2 h with a ball to powder ratio maintained at 1:10. YSZ was specifically mixed with mullite to improve the thermal cycling life of the coating, based on previous reports on the composite YSZ + mullite powder (Ref 15). 99.9% pure copper specimens of size 30 mm × 30 mm × 5 mm were used as substrates. This was in consideration of the actual tuyere material used in blast furnace applications.

2.2 Coating Deposition

As previously mentioned, both DSC and APS techniques were used for depositing all the coatings except YSZ. In view of the difficulty in obtaining practically relevant deposition rates with high melting point YSZ powders using DSC, this powder was applied through plasma spraying alone. In all cases, an identical bond coat of NiCoCrAlY was applied to a thickness of about 100-120 μm followed by a layer of the candidate coating to a thickness of 150-180 μm. Identical processes were employed for depositing both bond coat and top coat, i.e., either both were DSC sprayed or APS sprayed. The process parameters employed for DSC and APS coatings are indicated in Tables 1 and 2.

2.3 Coating Characterization

The coated specimens were sectioned using a slow speed Isomet cutting machine, and then mounted and polished for microscopic analysis. The cross-sectional microstructural features were observed using a scanning

Table 1 Process parameters used for DSC coatings

Powder identification	O ₂ flow rate, slph	C ₂ H ₂ flow rate, slph	Spray distance, mm	N ₂ powder carrier flow rate, slph
AZ	4960	2000	200	720
M	4800	1920	170	720
M-YSZ	4800	1920	200	720
CrC	2800	2240	170	720
NiCoCrAlY (Bond coat)	2720	2240	165	800

Table 2 Process parameters used for APS coatings

Powder	Primary gas flow rate, scfh	Current, A	Voltage, V	Standoff distance, mm
AZ	110	600	62-66	120
M	110	500	60-62	120
M-YSZ	110	510	60-62	80
YSZ	110	600	65-68	75
CrC	90	510	64-68	90
NiCoCrAlY	80	500	62-64	110

electron microscope (Model: S3400N, Hitachi, Japan). The Vickers microhardness was measured along the cross section of the coating using a digital microhardness tester (Model: VMH I04, UHL, Germany) with a load of 200 g. Porosity measurements on cross sections of coatings were carried out using image analysis software (analySIS software, Olympus GmbH, Germany). Microhardness and porosity values were measured at 10 locations, and the average values are reported herein. The phases present in the coating were identified using x-ray diffraction (XRD) analyses (Model: D8, Brukers AXS, Germany).

2.4 Evaluation of Erosion Performance of Coatings

Since erosion is known to be a contributor to tuyere degradation in actual operation (Ref 5), solid particle erosion tests were conducted on all coatings to rank their performance. Erosion testing was performed in dry sand erosion test rig at room temperature, with angular silica particles of size 50-150 μm impacting the substrates at a velocity of 40 m/s at angles of 30° and 90°. Feed rate of 2 g per minute was maintained during the test. After every 5 min of erodent impact, the weight loss was measured using a precision weighing balance and this was continued until steady-state values were observed. The measured weight loss was converted to volume loss using the appropriate coating density values and further reported in terms of volume loss per gm of erodent (cc/g). The above test was repeated on two sets of samples for each type of coating, and steady-state erosion values are reported herein.

2.5 Evaluation of Hot Corrosion Performance of Coatings

Corrosive gases like chlorine and sulfur emitted from burden material usually cause severe damage to the copper tuyere in service. Recognizing the role of corrosion in tuyere damage, all coatings were also subjected to corrosion testing. For this purpose, 50 wt.% FeCl_3 + 50 wt.% FeSO_4 salt was applied uniformly over the coating surface with coverage of 25 mg/cm^2 (Ref 9). Subsequently, the specimens were isothermally heated to 850 °C in a furnace (in air atmosphere) for 40 h and then cooled to room temperature, maintaining the heating and cooling rates at 3.5 °C/min. After testing, the samples were analyzed through XRD for determining changes in phase constitution.

2.6 Coating Behavior During Thermal Cycling

In actual operation, the tuyere nose often faces splashing of molten metal/slag, which is at temperature of about 1550 °C. This splashing of molten material raises the temperature of the tuyere nose to above 1000 °C (Ref 5), although the metal surface temperature is held at a significantly lower temperature (500-700 °C) because of instantaneous cooling due to the elaborate water cooling arrangement. This periodic increase and decrease in temperature is also one of the prime reasons for tuyere failure (Ref 5). Hence, it was deemed important to assess the behavior of coatings under thermal cycling conditions involving exposure to such high temperatures. Due to the obvious limitations in simulating such an environment in the laboratory by incorporating very efficient cooling in case of small coated specimens, thermal cycling tests were carried out with coatings generated over nickel-based super alloy substrates, on account of the limitation of inadequately cooled copper substrates to survive at temperatures as high as 1000 °C. The aim of this test was to solely assess the damage caused to coatings upon exposure to such temperature cycling. Six as-coated specimens generated using DSC and APS techniques were placed in alumina boats and were subjected to thermal cycling in a special furnace (Model: 1616, CM Furnaces, Bloomberg, USA). Each cycle comprised 20 min of heating to 1000 °C, followed by a 5 min hold, and subsequent 5 min cooling using a forced air draft to reach about 300 °C. The test was conducted for a maximum of 1000 cycles.

2.7 Field Testing of Coated Tuyere

After thorough property evaluation of the coating systems, a qualitative comparison of coatings was done to select the best coating material—coating process combination for an actual tuyere application. The coated tuyere was put in actual blast furnace operation, and its performance was evaluated in terms of increase in service life. The mode of failure for coated tuyere is proposed.

3. Results and Discussion

3.1 Coating Characteristics

3.1.1 Microstructure and Porosity. Figure 1 shows the cross-sectional micrographs of various detonation- and plasma-sprayed coatings. As observed in Fig. 1, the

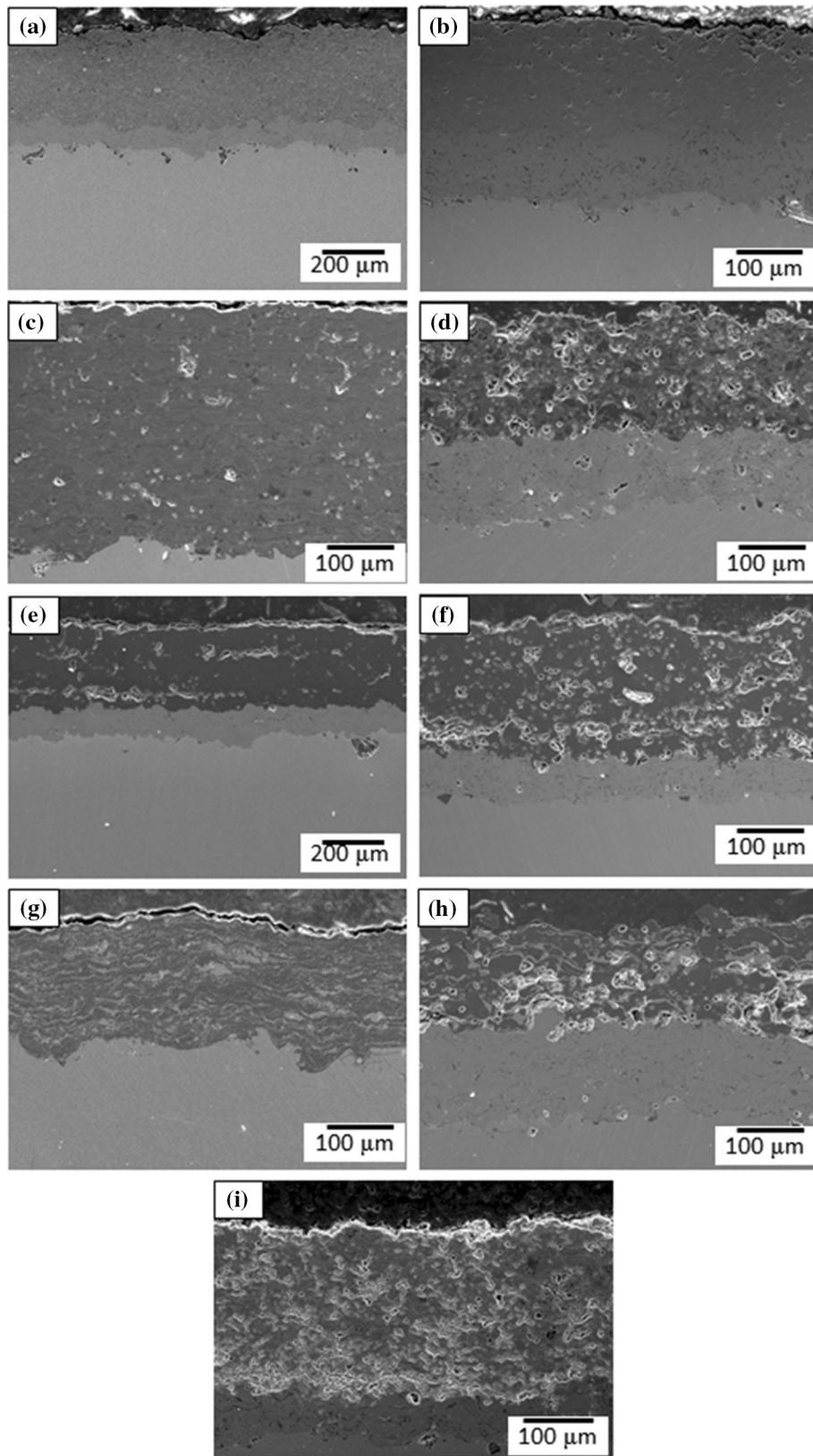


Fig. 1 Cross-sectional micrographs of (a) DSC-CrC, (b) APS CrC, (c) DSC-AZ, (d) APS-AZ, (e) DSC-M, (f) APS-M, (g) DSC M-YSZ, (h) APS M-YSZ, and (i) APS-YSZ coating

detonation-sprayed coatings showed denser microstructures than the plasma-sprayed equivalents for each coating material. The interface between the bond coat and the top coat also appeared sound in each case, without any cracks or delamination being visible.

Figure 2 shows the porosity measurements for all coatings. It was observed that DSC samples exhibited maximum porosity of 2% in case of AZ, while porosity values remained approximately 1% for all other coatings. APS-YSZ reported the highest porosity value of about 6%, followed by AZ, M, CrC, and M-YSZ. The plasma-sprayed coatings exhibited more than double of porosity values upon comparison with the detonation-sprayed coatings, which is typical of both the process.

3.1.2 Phase Constitution. The phase constitution of the various coatings as determined from XRD analyses is tabulated in Table 3. The effect of spraying technique is observed on the phase constitution of coatings. In case of DSC-M, it is observed that retention of the mullite phase in coating is difficult as compared to APS route. In DSC-M, γ -Al₂O₃ was observed as the major phase, while mullite and silica were the minor phases along with the amorphous nature observed at 25° (Ref 16). The latent heat, melting and evaporation temperatures of mullite are low, and hence, the decomposed mullite particles do not

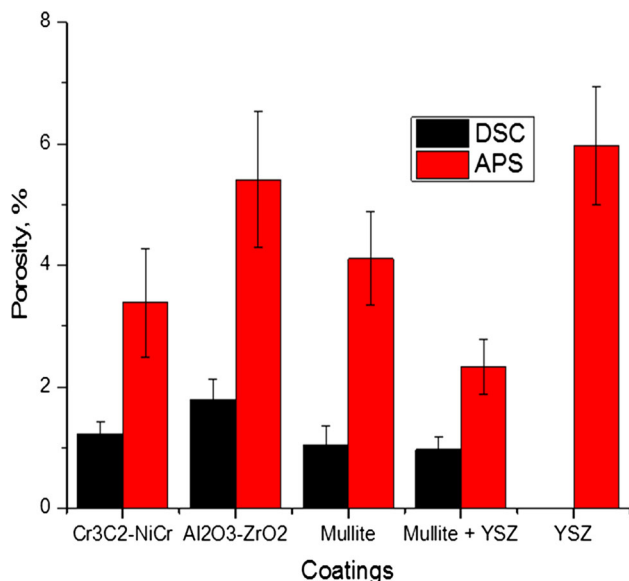


Fig. 2 Porosity values for DSC- and APS-sprayed coatings

get enough time to crystallize in DSC process due to intensive cooling on the substrate. This results in crystallizing of majority of γ -Al₂O₃ phase in DSC-M, while most of mullite phase is present in the form of amorphous phase (Ref 17). Similar observation was made for DSC M-YSZ coating also. Mullite phase was retained in small amount compared to APS M-YSZ. DSC and APS CrC coating shows the presence of same carbide phase constituents, while the binder material was identified as Cr_{1.12}Ni_{2.88} (Ref 18). Cr₃C₂ phase intensity was reduced in APS compared to DSC, indicating decarburization of the coating. In DSC-AZ, the coating shows retention of t' -ZrO₂ along with γ -Al₂O₃ as the major phase, while in APS-AZ, the coating shows additional presence of m -ZrO₂ as minor phase. Due to higher temperature in APS compared to DSC, there is a higher chance of phase transformation from tetragonal to monoclinic phase (Ref 17).

3.1.3 Microhardness of Coatings. In general, the microhardness values are a good indicator of inter-splat cohesive strength. However, the microhardness values are usually significantly lower than the corresponding bulk properties, due to inherent defects like porosity, voids, unmelted particles, etc., present in typical thermal-sprayed coatings. Among the various coatings studied, the relatively more porous nature of plasma-sprayed coatings is confirmed by the results of porosity measurements depicted in Fig. 2. This is, in turn, responsible for the reduced microhardness values in APS coatings as observed from Fig. 3.

For example, the CrC coating deposited by DSC exhibits higher hardness compared to the same coating deposited by APS, as the porosity is higher in the latter case as seen in Fig. 2. Higher magnification observation of CrC coating shows the distributed presence of hard chromium carbide particles in a NiCr matrix as shown in Fig. 4(a), while the APS CrC coatings show a lamellar structure with reduced presence of chromium carbide particles (Fig. 4b). This could be attributed to decarburization of carbide particles during high temperature exposure during plasma spraying as reported in previous studies (Ref 19).

The only exception to the above noted superiority of DSC microhardness values over those resulting from APS is the M-YSZ coating for which APS appears to be better suited than DSC. This is, in fact, consistent with the previously indicated difficulty of DSC in spraying YSZ because of the high melting point of the powder feedstock. As observed in Fig. 5(a) and (b), the relative degree of

Table 3 XRD analyses of coatings by DSC and APS route

Coating	Phases present in coating—DSC	Phases present in coating—APS
M	Major phase- γ -Al ₂ O ₃ , Minor phase-mullite and SiO ₂ , amorphous nature observed at 25°	Major phase-mullite, Minor phases- γ -Al ₂ O ₃ and SiO ₂ amorphous nature observed at 25°
M-YSZ	Major phase- t' -ZrO ₂ , Minor phase-mullite	t' -ZrO ₂ and mullite
CrC	Cr ₃ C ₂ , Cr ₂₃ C ₆ , Cr ₇ C ₃ , Nickel, Cr _{1.12} Ni _{2.88}	Minor phase-Cr ₃ C ₂ , Major phase-Cr ₂₃ C ₆ , Cr ₇ C ₃ , Nickel, Cr _{1.12} Ni _{2.88}
AZ	Major phase- γ -Al ₂ O ₃ , Minor phase- t' -ZrO ₂	Major phase- γ -Al ₂ O ₃ , Minor phases- t' -ZrO ₂ and m -ZrO ₂
YSZ		t' -ZrO ₂

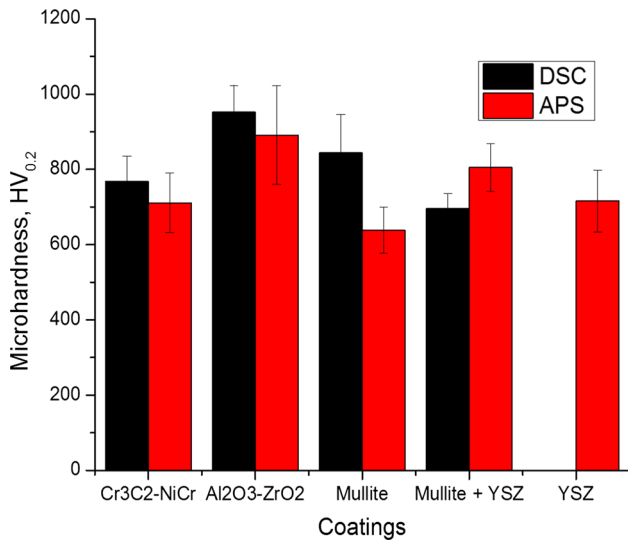


Fig. 3 Microhardness values for DSC- and APS-sprayed coatings

melting of APS-sprayed Mullite + YSZ coating was better than the DSC-sprayed equivalent. Also, pores and unmelted particles are visible in DSC M-YSZ cross section in Fig. 5(a).

As shown in Table 3, APS M-YSZ coatings comprise t' -ZrO₂ as the major phase along with minor amount of mullite, while the corresponding DSC sprayed coating is constituted of t' -ZrO₂, with only trace amount of the mullite phase. Greater extent of melting of the composite materials during plasma spraying could have resulted in better inter-splat adhesion yielding higher microhardness value. Even though significant amount of tetragonal zirconia is observed in both coatings, the possibilities of lesser degree of melting with the YSZ particles during DSC could have resulted in relatively lower hardness. Incidentally, the microhardness and porosity values match those reported for typical APS-YSZ coating (Ref 20).

DSC- and APS-sprayed AZ coatings exhibited highest hardness among all the coatings. The high hardness can be attributed to the presence of hard Al₂O₃ phase and further toughening of the microstructure by the zirconia phase (Ref 21).

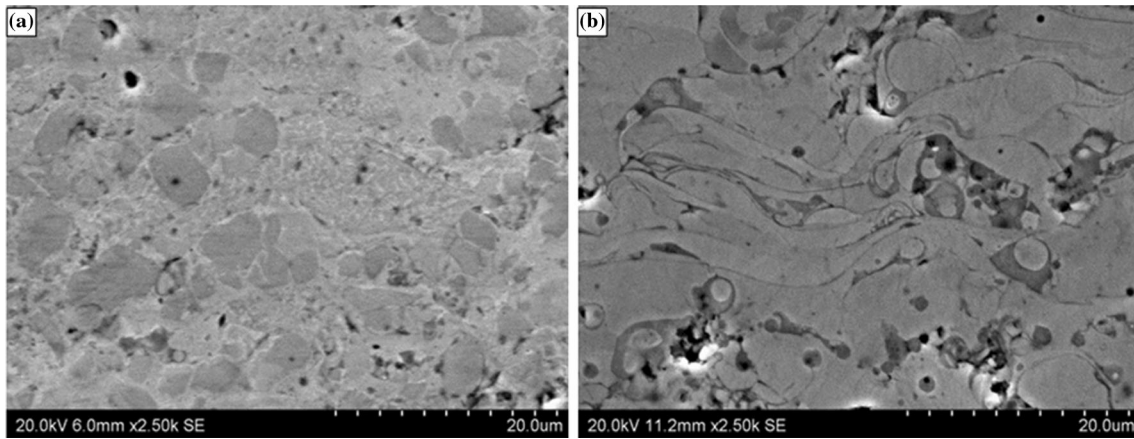


Fig. 4 CrC coating by (a) DSC route at higher magnification and (b) APS route at higher magnification

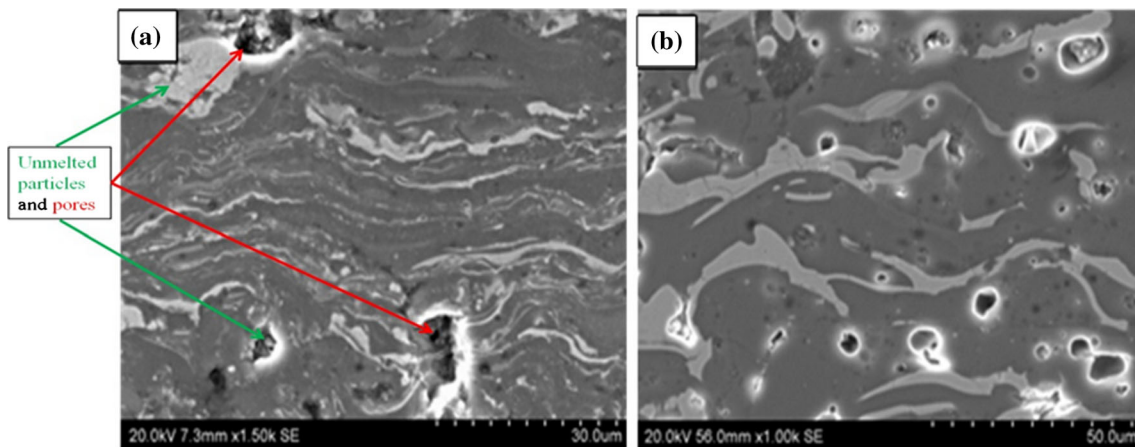


Fig. 5 High magnification cross-sectional images of (a) DSC M-YSZ and (b) APS M-YSZ

Mullite coating shows the second best hardness value through DSC route. However, it was lowest in terms of hardness among all the coatings generated by APS, it is observed that significant amount of silica is lost during DSC spraying, and the majority phase retained in the coating is the γ -Al₂O₃ phase, as shown in Table 3. Also, a hump was observed around 25° indicating the presence of an amorphous phase in the detonation-sprayed coating. The higher hardness observed with DSC mullite can be attributed to γ -Al₂O₃ and amorphous phases. Interestingly with the APS route, the coating shows good retainment of mullite phase, which possibly accounted for relatively lower hardness values. Similar values as determined in this study for APS mullite coatings have also been previously reported and are typical of the presence of mullite phase alone (Ref 20).

3.2 Erosion Performance of Coatings

The erosion test was performed at various impact angles and at higher impact velocities to assess effectiveness of the coatings. The test method provides the extent of material loss due to impact by gas-entrained solid silica particles at pre-determined angles and velocities. The erosion wear performance of the DSC and APS coating is summarized in Fig. 6 and 7.

The data presented above are in terms of volumetric loss incurred by the coating per gram of erodent impacting the coated surface. The reported volumetric loss is meaningful in order to compare materials with different densities. The density values used for the above studies were mullite-3.2 g/cc, mullite + YSZ-3.6 g/cc, Al₂O₃-ZrO₂-4.2 g/cc, Cr₃C₂-NiCr-6.9 g/cc, YSZ-5 g/cc as measured using the widely adopted Archimedes' method (Ref 22).

From the above results, it is clear that coatings synthesized by the DSC route show much superior erosion resistance compared to the APS coatings. This is to be expected in view of the consistently lower porosity and, in most cases, higher hardness exhibited by the DSC coatings as previously discussed. In addition to the above, it is also well documented in the literature as well as in studies published from the authors' laboratory that the optimum particle temperature and higher particle velocity enable detonation-sprayed coatings to exhibit compressive residual stresses (Ref 14, 23). The compressive nature of residual stress also is found to improve adhesion characteristics and mechanical properties (Ref 23-27). A wide range of coatings, including ceramics, alloy or cermet coatings, deposited by the detonation spray technique have been found to yield compressive stresses which, in turn, manifested in the form of enhanced wear resistance, fatigue life, etc., compared to other techniques (Ref 23, 25-27).

CrC coatings exhibited highest erosion resistance compared to other coatings, mainly due to the presence of NiCr binder which acts as a toughening agent in absorbing the impact force and also due to the chromium carbide network of hard particles, restricting the propagation of cracks (Ref 28). Among the different ceramic materials,

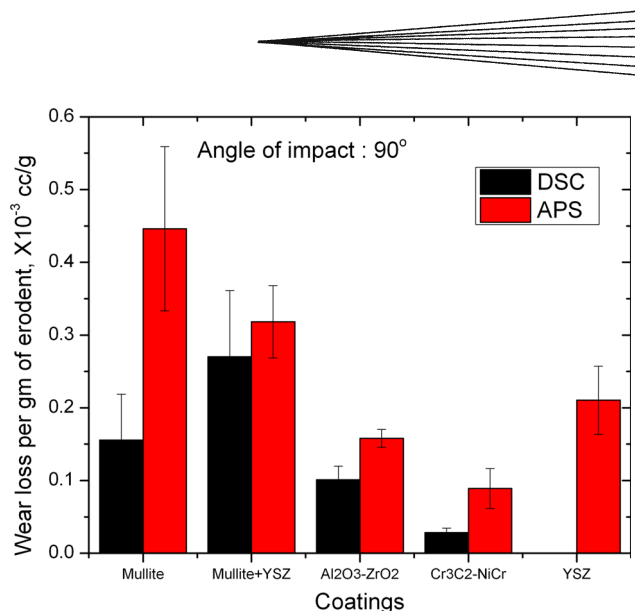


Fig. 6 Erosive wear performance of DSC and APS coatings tested at an impact velocity of 40 m/s at impact angle of 90°

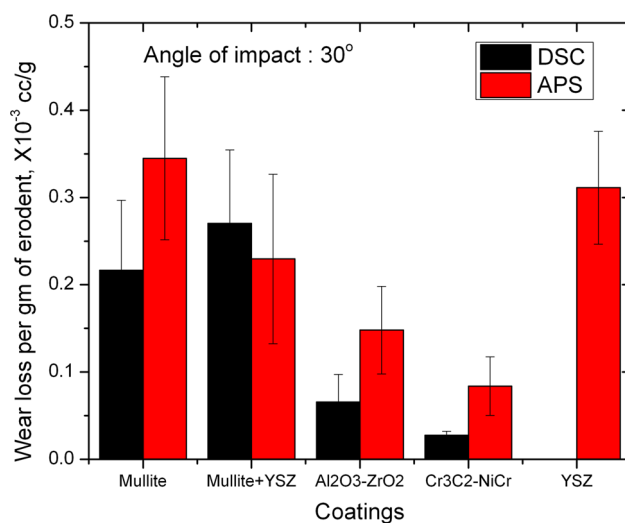


Fig. 7 Erosive wear performance of DSC- and APS-sprayed coatings tested at an impact velocity of 40 m/s and at impact angle of 30°

AZ generated by both DSC and APS showed the best performance and this can plausibly be attributed to toughening of alumina by zirconia within the coating microstructure. The role of zirconia in improving the toughness of alumina has been shown by Claussen (Ref 29) in sintered material. Also, Wang et al. (Ref 30) have shown that zirconia toughened alumina ceramics show nearly four times higher toughness compared to alumina, which is a significant factor in improving erosion resistance. However, it is observed that the YSZ coating shows relatively higher wear rate due to its higher porosity and lower microhardness, besides its reportedly low fracture toughness (Ref 31). Higher relative wear loss for M and

Table 4 Phase analysis of APS- and DSC-coated specimens before and after hot corrosion

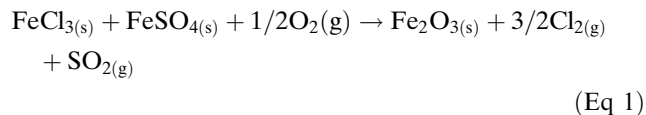
Coating system	Phases present in as-coated condition	Phases present after hot corrosion
M (DSC, APS)	Mullite, γ -Al ₂ O ₃ , SiO ₂	Mullite, γ -Al ₂ O ₃ , SiO ₂ , Fe ₂ O ₃
M-YSZ (DSC, APS)	Mullite, t' -ZrO ₂	Mullite, t' -ZrO ₂ , Fe ₂ O ₃
AZ (DSC)	γ -Al ₂ O ₃ , t' -ZrO ₂	γ -Al ₂ O ₃ , t' -ZrO ₂ , Fe ₂ O ₃
AZ (APS)	γ -Al ₂ O ₃ , t' -ZrO ₂ , m -ZrO ₂	γ -Al ₂ O ₃ , t' -ZrO ₂ , m -ZrO ₂ , Fe ₂ O ₃
CrC (DSC, APS)	Cr ₃ C ₂ , Cr ₂₃ C ₆ , Cr ₇ C ₃ , Cr _{1.12} Ni _{2.88}	Cr ₂ O ₃ , Fe ₂ O ₃ , NiO, Fe ₂ O ₃
YSZ (APS)	t' -ZrO ₂	t' -ZrO ₂ , Fe ₂ O ₃

M-YSZ coating can be attributed to higher porosity and lower flexural strength and elastic modulus for mullite phase (Ref 32). In mullite-based coatings, M and M-YSZ, deposited by DSC route, exhibited lower wear loss compared to APS-based coatings. Apart from the comparatively lower porosity in the DSC deposited coatings compared to the APS coatings, the presence of hard alumina and t' -ZrO₂ phases in detonation-sprayed M and M-YSZ coatings, respectively, could have also contributed to their superior erosion resistance compared to the corresponding APS coatings.

The results depicted in Fig. 6 and 7 also enable comparison of the effect of impact angle on wear loss. In all coating systems except YSZ and mullite-based coatings sprayed by DSC, the maximum wear loss is observed at 90° impact than at 30°, which is in agreement with the findings of Lidija et al. (Ref 33).

3.3 Hot Corrosion Studies

The hot corrosion performance of the DSC and APS coatings is another important criterion to qualify the coatings for the desired applications. After an exposure of 40 h to corrosive species, the phase analysis of coatings was carried out to assess the extent of degradation. The phases present in the coatings before and after the test are summarized in Table 4. It is pertinent to note that alumina, zirconia, YSZ, and mullite are known for their resistance to hot corrosion by 'S' and 'Cl' species (Ref 34-36). During the course of exposure to 40 h, no spallation was observed in the ceramic coatings. Consistently for all the coatings, an additional peak of Fe₂O₃ forms due to the following reaction of corrosive salt applied over the coating:



Phase analysis of CrC coating after hot corrosion indicated formation of Cr₂O₃. Earlier studies have reported that 'Cr' reacts with oxygen in air and results in the formation of Cr₂O₃ (Ref 37). After exposure to hot corrosion testing conditions, one can observe from Table 4 that all the chromium carbide phases detected in the as-coated condition have dissociated and resulted into Cr₂O₃ formation. Also, through visual examination, it was observed that the green-colored Cr₂O₃ film had spalled-off from the surface, which can be seen in Fig. 8. After hot corrosion testing, the absence of hard carbide phases and the presence of

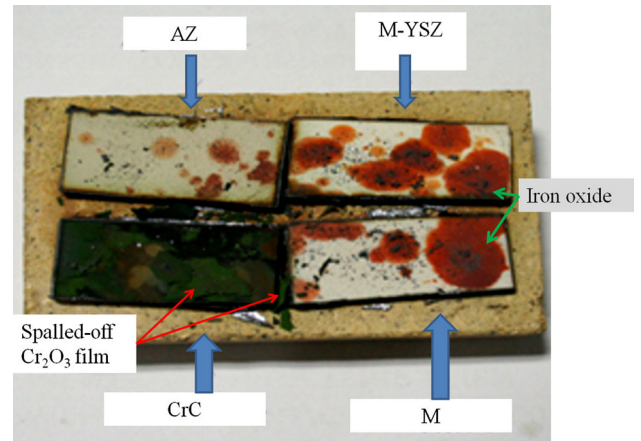


Fig. 8 DSC samples after hot corrosion test

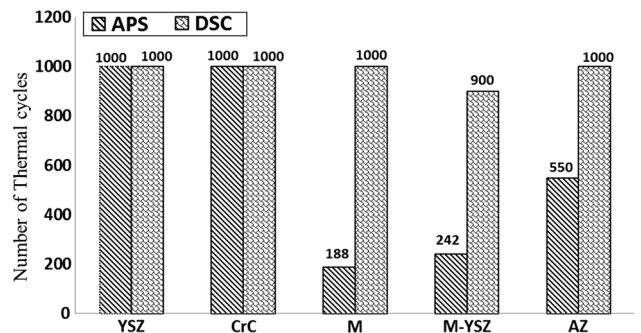


Fig. 9 Thermal cycling behavior of coatings

non-adherent Cr₂O₃ film show the poor hot corrosion behavior of CrC coating. Though CrC coatings exhibited better microhardness and improved erosion resistance properties, their poor hot corrosion resistance makes the coating inappropriate for tuyere application.

3.4 Thermal Cycling Studies

The spalling resistance of coatings was assessed through thermal cycling tests carried out. The test was terminated after 1000 cycles, and any noted failure prior to termination of the test is shown in Fig. 9. Among the coatings studied, all DSC-sprayed coatings withstood 1000 cycles of exposure without spallation, except for M-YSZ

which spalled at around 900 cycles. On the other hand, in case of plasma-sprayed coatings, CrC and YSZ coatings alone survived for 1000 cycles. The performance of all the other APS coatings could be categorized as inadequate: the mullite coatings spalled after 135-240 cycles, M-YSZ withstood for only about 215-270 cycles, and AZ lasted up to a modest 440-660 cycles.

The poor thermal cycling life of APS-sprayed mullite coating can be attributed to coefficient of thermal expansion mismatch (Ref 38). The corresponding DSC-sprayed coating was mostly amorphous, which could have assisted in extending the thermal cycling life up to 1000 cycles. Similarly, as mentioned in Table 3, the presence of

mullite in APS-sprayed M-YSZ coating could have resulted in lower thermal cyclic life. On the other hand, the DSC-sprayed M-YSZ coating showed predominant presence of t' -ZrO₂ as the major phase which resulted in improved thermal cycling life of 900 cycles. Both DSC- and APS-sprayed CrC coatings withstood 1000 thermal cycles. The top surface of the CrC coatings exhibited a greenish color implying that the surface had transformed to Cr₂O₃ in case of both DSC and APS coatings. This is similar to the previously reported findings of Kamal et al. (Ref 39). YSZ also has a high CTE value ($-11 \times 10^{-6} \text{ K}^{-1}$) (Ref 34) which is reportedly beneficial in reducing the thermal stresses arising between the underlying bond coat and the

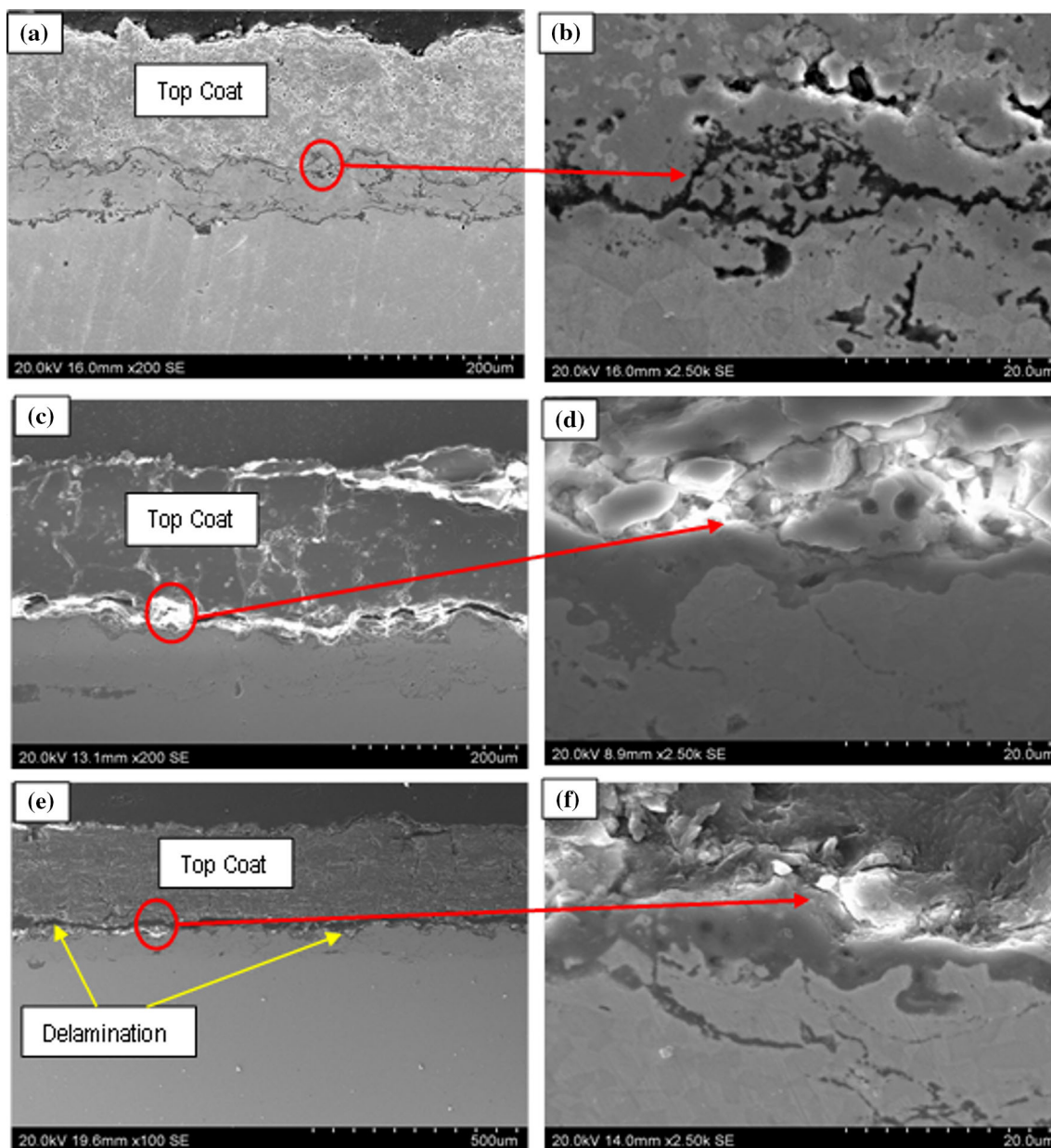


Fig. 10 Typical cross-sectional micrographs of DSC samples after thermal cycling test (a) CrC at lower magnification, (b) CrC at higher magnification (c) M—at lower magnification (d) M—at higher magnification, (e) M-YSZ—at lower magnification, and (f) M-YSZ—at higher magnification

top coat of YSZ during thermal cycling. Similar to most TBCs, APS-YSZ coatings withstood the 1000 cycles of test without any spallation.

Cross-sectional analysis of some DSC sprayed coatings was also carried out to understand the oxidation/failure mechanism. CrC coatings deposited by DSC showed less oxidation at the interface between top coat and bond coat as observed in Fig. 10(a). The interface remained intact (Fig. 10b), although some horizontal cracks were observed. The DSC sprayed mullite (Fig. 10c, d), on the other hand, showed extensive oxidation along with considerable but discontinuous cracking in the vicinity of the oxide scale. However, the mullite coating may have remained attached to the underlying bond coat due to the presence of regions that remained free of crack to survive during thermal cycling. The M-YSZ coating showed (Fig. 10e, f) significant oxidation at the interface and extensive horizontal cracking within the microstructure, which could have eventually led to its failure at around 900 cycles.

3.5 Field Evaluation of Coating

After thorough evaluation of coating characteristics and performance under different simulated environments, a suitable coating system was chosen for the perceived tuyere application using the qualitative comparison of all coatings as shown in Table 5. It becomes clear from Table 5 that AZ is clearly an unambiguous choice as coating material. DSC and APS sprayed AZ coatings have performed well in almost all the tests. APS-AZ performed inferior to DSC-AZ in erosion testing, while APS-AZ performed superior compared to DSC-AZ in thermal cycling. CrC coating could have been a very good choice of material, except that it performed extremely poor in hot corrosion test, rendering it unsuitable for the application. Even though APS-YSZ performed poorly in microhard-

ness and erosion tests, its hot corrosion and thermal cycling performance were excellent. Also, YSZ has higher coefficient of thermal expansion compared to AZ, hence it was decided to reinforce the coating system with an intermediate layer of YSZ with a view to enhance the overall performance of the coating system. The following two coating material-coating process combinations appear to be equally promising solutions for tuyere application. (1) APS-NiCoCrAlY bond coat, APS-YSZ intermediate coat, and DSC-AZ top coat. (2) APS-NiCoCrAlY bond coat, APS-YSZ intermediate coat and APS-AZ top coat. The second combination was selected for plant trial due to widespread global availability of APS compared to DSC, to address a problem faced by the steel industry worldwide.

Accordingly, an actual tuyere was APS coated with the following specifications: Bond coat of NiCoCrAlY with thickness 100 μm , intermediate ceramic coat of YSZ with coating thickness of 150 μm , and ceramic top coat of AZ with coating thickness of 150 μm . The as-coated tuyere is shown in Fig. 11(a). After continuous monitoring of the tuyere performance, a 90% improvement in service life was demonstrated using the coating. The disassembled coated tuyere (Fig. 11b) shows signs of mixed mode of failure, i.e., thermal loading, erosion, and corrosive gas attack. The YSZ and AZ coatings are known to be resistant to the possible corrosive gas attack as understood from the simulated studies. Therefore, the failure of top ceramic layers can be attributed to the thermal loading and erosion attack. It is believed that the top ceramic layers might have resisted erosion and thermal damage for long time before being eventually removed due to impact. One top layers failed, the bond coat and the underlying copper substrate might have failed at a faster rate leading to the complete failure. Figure 11(b) also shows that the bottom part of the nose has higher degree of damage on account of thermal loading, while the top surface and sides

Table 5 Qualitative comparison of all coating systems (Color table online)

Property / Testing	Qualitative ranking of coating (1 = best, 9 = worst)								
	1	2	3	4	5	6	7	8	9
Microhardness	DSC - AZ	APS - AZ	DSC - M	APS M-YSZ	DSC - CrC	APS - CrC	DSC M-YSZ	APS - YSZ	APS - M
Erosion at 90 degree impact angle	DSC - CrC	DSC - AZ	APS - CrC	APS - AZ	DSC - M	APS - YSZ	DSC M-YSZ	APS M-YSZ	APS - M
Erosion at 30 degree impact angle	DSC - CrC	DSC - AZ	APS - CrC	APS - AZ	DSC - M	APS M-YSZ	DSC M-YSZ	APS - YSZ	APS - M
Hot corrosion	DSC - AZ, APS - AZ, DSC - M, APS - M, APS M-YSZ, DSC M-YSZ, APS - YSZ								DSC - CrC, APS - CrC
Thermal Cycling	APS - AZ, APS - M, APS - YSZ, DSC - CrC, APS - CrC					APS M-YSZ	DSC - AZ	DSC M-YSZ	DSC - M

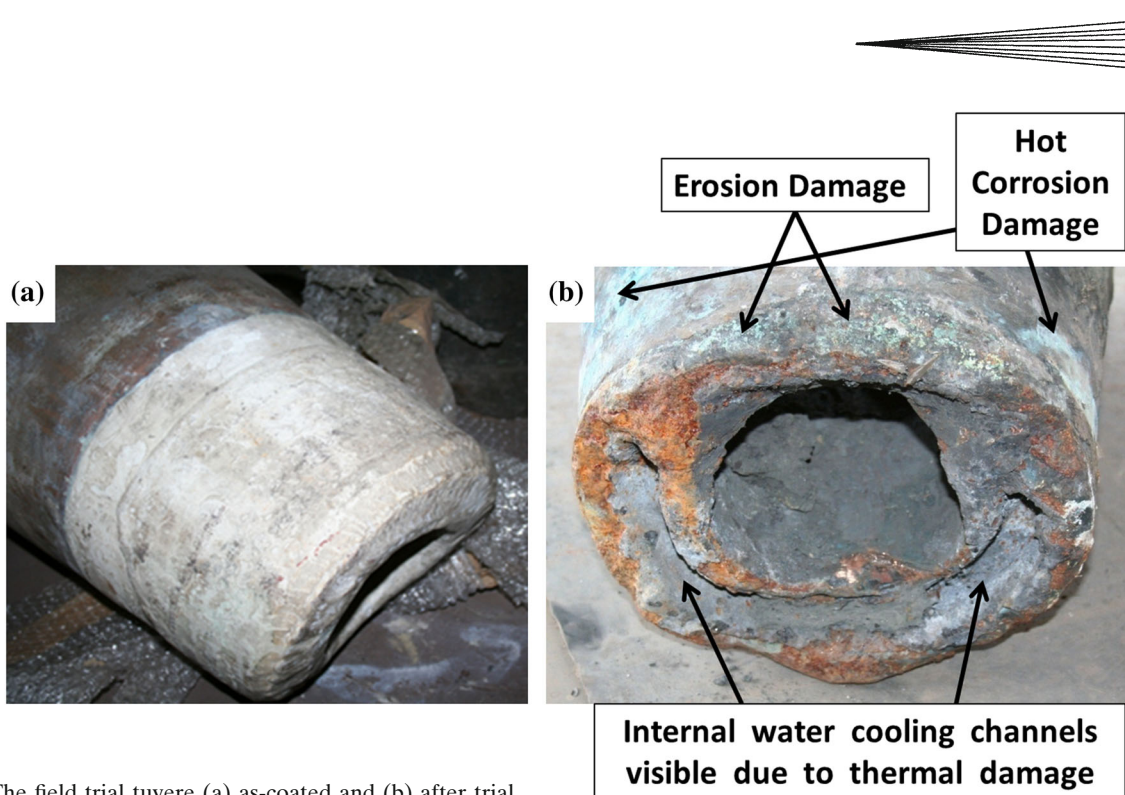


Fig. 11 The field trial tuyere (a) as-coated and (b) after trial

of tuyere nose compelled to failure under signs of erosion damage and hot corrosion attack.

4. Conclusion

Various ceramic and cermet coatings were applied on a copper substrate using DSC and APS techniques to explore their performance for possible blast furnace tuyere applications. Although CrC coatings exhibited high microhardness and erosion resistance, their poor performance in hot corrosion conditions makes the coating inappropriate for actual application. M and M-YSZ coatings also showed poor microhardness and thermal cycling results, rendering them unsuitable. The APS and DSC-AZ coatings exhibited highest microhardness and were inert to hot corrosion attack. While the DSC-AZ coating exhibited very good thermal cycling performance, the APS-AZ coating even survived for a modest number of thermal cycles prior to failure, suggesting that it could be a possible candidate for the intended tuyere application. The YSZ coatings showed best thermal barrier property sustaining 1000 thermal cycles without failure and displayed moderate microhardness and erosion resistance property. In view of the above, a combination of AZ and YSZ coatings was deemed suitable to mitigate the three modes of failure observed in tuyeres, i.e., erosion damage, thermal loading, and hot corrosion. Accordingly, NiCoCrAlY bond coat, AZ intermediate coat, and YSZ top coat were deposited using APS. The applicability of the selected coating system was successfully demonstrated in field trial with an improvement in service life by 1.9 times.

References

1. C. Copeland and S. Street, A Practical Engineering Approach to Improving the Reliability of Blast Furnace Tuyeres, *Iron Steel Technol.*, 2013, p 47-62
2. S. Matthews and B. James, Review of Thermal Spray Coating Applications in the Steel Industry: Part-1 Hardware in Steel Making to the Continuous Annealing Process, *J. Therm. Spray Technol.*, 2010, **19**(6), p 1267-1276
3. J. Hartman, Notes on Tuyeres in the Iron Blast Furnace, *Trans. Am. Inst. Min. Eng.*, 1898, **28**, p 666-673
4. T. Shellhammer and R. Walsh, High Conductivity Copper in the Blast Furnace, *AISTech Conference Proceedings*, 2010, I, p 437-452
5. Anon., The Explosion of No. 5 Blast Furnace, Corus UK Ltd., Port Talbot, United Kingdom, *Health and Safety Executive Report*, UK, 2001, p 47
6. Y. Zhao, M. Atkinson, H. Crosman, C. Tetrault, D. Roldan, and C. Zhou, Investigation of Tuyere Nose Failures at U. S. Steel—Great Lakes Works B2 Blast Furnace, *AISTech Conference Proceedings*, 2005, I, p 491-496
7. H. Nakahira, Blast-Furnace Tuyere Having Excellent Thermal Shock Resistance and High Durability, US3977660 A, 1976
8. H. Watanabe, S. Shoji, A. Sato, and T. Oka, Blast-Furnace Tuyere, US4189130 A, 1980
9. H. Fukubayashi, Metal-Zirconia Composite Coating, International Patent, Publication Number WO 02/075004 A1. Praxair S.T. Technology Ltd., 2002
10. D. Yang, Y. Guan, Y. Zhang, J. Li, J. Hu, and W. Li, Application of Ceramic Coat Synthesized by In-Situ Combustion to BF Tuyere, *J. Iron Steel Res. Int.*, 2007, **14**(2), p 70-72
11. Y. Ohmae, Surface Coated Blast Furnace Tuyere Made of Copper or Copper Alloy and Method of Surface Coating the Same, US4139673, 1979
12. H. Yamaoka, M. Kawasaki, H. Kawanami, T. Shiino, and J. Yamashita, Tuyers for a Blast Furnace, US4043542, 1977
13. J. Song, T. Wang, J. Yuan, L. Zhang, and X. Tan, Tuyeres of Blast Furnace Surface Recombination Coating and Method for Preparing the Same, Publication Number CN101492749 (A). Baoshan Iron and Steel (CN), 2009

14. G. Sundararajan, D. Srinivasa Rao, G. Sivakumar, and S.V. Joshi, in *Detonation Spray Coatings*, ed. by J. Wang, W. Chung, Encyclopedia of Tribology, 1st ed. (Springer, US, 2013), p 736-742
15. E. Withey, C. Peorak, R. Trice, G. Dickinson, and T. Taylor, Design of 7 wt% Y_2O_3 - ZrO_2 /Mullite Plasma Sprayed Composite Coatings for Increased Creep Resistance, *J. Eur. Ceram. Soc.*, 2007, **27**, p 4675-4683
16. M.M. Hossen, F.U.Z. Chowdhury, M.A. Gafur, A.K.M. Abdul Hakim, and S. Nasrin, Investigation of Mechanical Properties of Al_2O_3 -20 wt % ZrO_2 Composites as a Function of Sintering Temperature, *Eur. Sci. J.*, 2014, **10**(9), p 399-411
17. H. Tahara, M. Moriyama, and K. Fujiuchi, Ceramic Spraying Using Electromagnetically Accelerated Plasma, *Proceedings of International Thermal Spray Conference, Osaka, Japan*, 2004, p 612-618
18. N.L. Parthasarathi and M. Duraiselvam, Improvement of High Temperature Wear Resistance of AISI, 316 ASS Through NiCrBSiCFe Plasma Spray Coating, *J. Min. Mater. Charact. Eng.*, 2010, **9**(7), p 653-670
19. M.W. Richert, M. Książek, P. Pałka, S. Wawrzyniak, R. Grzelka, and K. Płońska-Niżnik, Microstructure Characterization of Chromium Carbide Coatings Deposited by Thermal Spray Processes, *J. Achiev. Mater. Manuf. Eng.*, 2012, **55**(1), p 108-112
20. L. Pawlowski, *Properties of Coatings, The Science and Engineering of Coatings*, 2nd ed. (John Wiley & Sons Ltd, 2008), p 399-400
21. A.A. Abdel-Samad, A.M.M. El-Bahloul, E. Lugscheider, and S.A. Rassoul, A Comparative Study on Thermally Sprayed Alumina Based Ceramic Coatings, *J. Mater. Sci.*, 2000, **35**(12), p 3127-3130
22. N. Margadant, S. Siegmann, J. Patscheider, T. Keller, W. Wagner, J. Ilavsky, J. Pisacka, G. Barbezat, P. Fiala, and T. Pirling, Microstructure—Property Relationships and Cross-Property-Correlations of Thermal Sprayed Ni-Alloy Coatings, *Proceedings of Thermal Spray 2001—New Surfaces for New Millennium, Singapore*, 2001, p 643-652
23. G. Sundararajan, D. Sen, and G. Sivakumar, The Tribological Behavior of Detonation Sprayed Coatings: The Importance of Coating Process Parameters, *Wear*, 2005, **258**(1), p 377-391
24. W. Tie-Gang, Z. Sheng-Sheng, H. Wei-Gang, L. Jia-Bao, G. Jun, and S. Chao, Estimation of Residual Stress and Its Effects on the Mechanical Properties of Detonation Gun Sprayed WC-Co Coatings, *Mater. Sci. Eng. A*, 2010, **527**(3), p 454-461
25. B. Rajasekaran, S. Sundara Raman Ganesh, V. Joshi, and G. Sundarajan, Performance of Plasma Sprayed and Detonation Gun Sprayed Cu-Ni-In Coatings on Ti-6Al-4V Under Plain Fatigue and Fretting Fatigue Loading, *Mater. Sci. Eng. A*, 2008, **479**(1-2), p 83-92
26. J.K.N. Murthy and B. Venkataraman, Abrasive Wear Behavior of WC-CoCr and Cr_3C_2 -20(NiCr) Deposited by HVOF and Detonation Spray Processes, *Surf. Coat. Technol.*, 2006, **200**(8), p 2642-2652
27. G. Sivakumar, L. Ramakrishna, V. Jain, D. Srinivasa Rao, and G. Sundararajan, The Influence of the Process Parameters on the Properties of Detonation Sprayed WC-12Co Coatings, *Proceedings of International Thermal Spray Conference. ASM Materials*, 2001, p 1031-1038
28. D. Toma, W. Brandl, and G. Marginean, Wear and Corrosion Behaviour of Thermally Sprayed Cermet Coatings, *Surf. Coat. Technol.*, 2001, **138**(2-3), p 149-158
29. N.J. Claussen, Fracture Toughness of Al_2O_3 with an Unstable ZrO_2 Dispersed Second Phase, *J. Am. Ceram. Soc.*, 1976, **61**, p 49-51
30. J. Wang and R. Stevens, Review Zirconia-Toughened Alumina (ZTA) Ceramics, *J. Mater. Sci.*, 1989, **24**, p 3421-3440
31. J.R. Davis, Ed., *Handbook of Thermal Spray Technology* (ASM International, Materials Park, OH, 2004), p 158
32. W.D. Callister Jr., *Structure and Properties of Ceramics, Materials Science and Engineering: An Introduction*, 6th ed. (John Wiley & Sons Ltd, 2009), p 399-400
33. Lidija. Čurković, Ivan. Kumić, and Krešimir. Grilec, Solid Particle Erosion Behaviour of High Purity Alumina Ceramics, *Ceram. Int.*, 2011, **37**(1), p 29-35
34. W. Gao and Z. Li, Eds., *Developments in High-Temperature Corrosion and Protection of Materials* (Woodhead Publishing-CRC press, Cornwall, England), p 499
35. C. Ramachandra, K.N. Lee, and S.N. Tewari, Durability of TBCs with a Surface Environmental Barrier Layer Under Thermal Cycling in Air and in Molten Salt, *Surf. Coat. Technol.*, 2003, **172**, p 150-157
36. A. Keyvani, M. Saremi, and M.H. Sohi, Microstructural Stability of Zirconia-Alumina Composite Coatings During Hot Corrosion Test at 1050°C, *J. Alloys Compd.*, 2009, **506**(1), p 103-108
37. S. Sen, O. Ozdemir, A.S. Demirkiran, and U. Sen, Oxidation Kinetics of Chromium Carbide Coating Produced on AISI, 1040 Steel by Thermo-Reactive Deposition Method during High Temperature in Air, *Adv. Mater. Res.*, 2012, **445**, p 649-654
38. K.N. Lee, R.A. Miller, and N.S. Jacobson, New Generation of Plasma-Sprayed Mullite Coatings on Silicon Carbide, *J. Am. Ceram. Soc.*, 1995, **78**(3), p 705-710
39. S. Kamal, R. Jayaganthan, and S. Prakash, High Temperature Oxidation Studies of Detonation-Gun-Sprayed Cr_3C_2 -NiCr Coating on Fe- and Ni-Based Superalloys in Air Under Cyclic Condition at 900°C, *J. Alloys Compd.*, 2009, **472**, p 378-389